Physics – Uspekhi **61** (11) 1100 – 1115 (2018)

CONFERENCES AND SYMPOSIA

PACS numbers: 03.65.Nk, 03.65.Xp, **85.35. – p**, **85.65. + h**

Quantum logic gates

A A Gorbatsevich, N M Shubin

DOI: https://doi.org/10.3367/UFNe.2017.12.038310

Contents

Abstract. **We discuss the strategies to construct logic gates based on solid-state and molecular structures in which information transformation processes are governed by quantum mechanical principles and which, similarly to the classical complementary metal–oxide–semiconductor (CMOS) structures, do not consume power in the stationary state. In the first-generation quantum analogs of CMOS gates, logical state switching occurs by fast quantum mechanical tunneling processes, but the transfer characteristics are determined by classical diffusion–drift carrier transport. The second-generation quantum analogs of CMOS systems are open quantum systems in which charge carrier transport occurs coherently. The development of atomic-precision lithography will allow wide use of quantum molecular logic gates in traditional computer architectures.**

Keywords: quantum transport, resonant tunneling, quantum interference, non-Hermitian Hamiltonian, *PT* symmetry, exceptional point, coalescence of resonances, logic gate, complementary metal–oxide–semiconductor (CMOS) transistor, quantum inverter, switching voltage, transfer characteristics, nanoelectronics, molecular electronics

A A Gorbatsevich Lebedev Physical Institute,
Russian Academy of Sciences,
Leninskii prosp. 53, 119991 Moscow, Russian Federation
E-mail: aagor137@mail.ru, aag.qdn@miee.ru
N M Shubin Lebedev Physical Institute, Russian Academy of Sciences,
Leninskii prosp. 53, 119991 Moscow, Russian Federation;
Moscow State Institute of Electronic Technology (Technical University),
pl. Shokina 1, 124498 Zelenograd, Moscow, Russian Federation
E-mail: n.s.vanderveer@gmail.com

Received 13 December 2017
Uspekhi Fizicheskikh Nauk **188** (11) 1209 – 1225 (2018)
DOI: https://doi.org/10.3367/UFNr.2017.12.038310
Translated by M L Skorikov; edited by A M Semikhatov

1. Introduction

Modern electronics are based on CMOS circuits, whose architecture is based on a pair of complementary metal–oxide–semiconductor (MOS) transistors with a common input [1]. In a stationary state at a given input voltage (Fig. 1), one transistor is open and the other is closed. This can be implemented naturally if the complementary pair consists of a p-type and an n-type transistor. An electric circuit implementing a logic function is conventionally called a gate. Figure 1 shows the NOT gate (an inverter), which is obtained if in addition to the common input, the transistors in the CMOS pair have a common output. A logic gate is typically loaded by another logic gate, where the input voltage is applied to the gates of the transistors in the CMOS pair, which are electrically isolated from their channels. Hence, the output resistance of a logic gate is extremely high, and the current flowing through the circuit is determined by leakage across the gates of MOS transistors, which is very low. Therefore, the voltage at the output of a logic gate is determined by the reference voltage of the open transistor in the CMOS pair.

The reference voltages in the inverter circuit are chosen such that for an input voltage $V_{\text{in}} = V_{\text{ref2}}$, the transistor with the reference voltage V_{ref1} is open (and therefore the transistor with the reference voltage is V_{ref2} is closed). Then the output voltage of the inverter equals V_{ref1}. Likewise, for the input voltage $V_{\text{in}} = V_{\text{ref1}}$, the output voltage equals V_{ref2}. By assigning the logic levels 0 and 1 to the values of the reference voltages V_{ref1} and V_{ref2}, we find that the circuit performs the logic NOT operation. Most frequently, the reference voltages V_{ref1} and V_{ref2} are the zero (ground) and the power supply voltages.

By combining the inputs and outputs of CMOS transistors in certain ways, it is possible to implement any logic function [2]. It is highly important that the current flowing

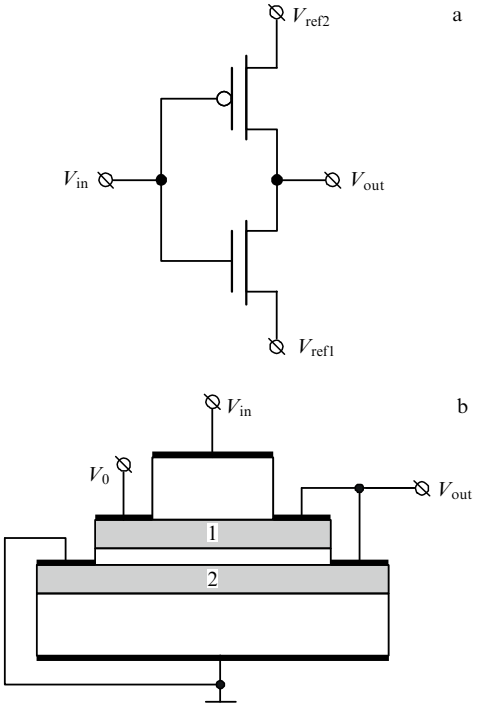

Figure 1. (a) Circuit diagram of a CMOS inverter. (b) Layout of a double-well quantum inverter. GaAs quantum wells are shown in gray. Reference voltages V_{ref1} and V_{ref2} are set by the ground bus potential ($V_{ref1} = 0$) and the supply voltage potential ($V_{ref2} = V_0$).

through a CMOS element in a stationary state is extremely low and therefore the power consumption of CMOS circuits is also very low. This explains their dominance in modern electronics, which are progressing towards the development of more and more complex integrated circuits with an ever increasing scale of integration and currently featuring up to several billion transistors.

The switching of a transistor in a CMOS pair from the open to the closed state (and vice versa) is carried out by changing the concentration of charge carriers in the transistor channel, which, in turn, is achieved via classical drift and diffusion processes resulting in a redistribution of charge carriers between the channel and the drain/source of the transistor, as well as the bulk.

A novel class of semiconductor devices representing quantum analogues of CMOS circuits where switching takes place via the controlled relocation of the maximum of the absolute value of the electron wave function between tunneling-coupled quantum wells was proposed and investigated in a series of publications by Kopaev and coauthors [3–6]. In this approach, information is carried by the amplitude of the electron wave function in a certain region of a quantum system: the maximum and minimum of this amplitude respectively correspond to the logic 1 and 0. The application of an external voltage to the structure results in controlled relocation of the electron density in the system, corresponding to some transformation of the data according to the desired law.

Physically, the implementation of the suggested devices that use the principle of controlled electron density relocation is based on semiconductor heterostructures with coupled quantum wells. The design of a quantum analogue of the CMOS gate is basically similar to that of a classical device (see Fig. 1) dissected along the plane dividing the complementary transistors, with the resulting halves joined such that the channels of the two transistors are tunnel coupled. The quantum analogues of CMOS circuits discussed in [3–6] constituted one of the first proposals to meet the demand for increasing the density of elements on a chip by the use of a vertical three-dimensional (3D) arrangement. Currently, the 3D arrangement is already widely used in memory devices [7] and is considered one of the most promising areas for the advancement of the basic components. The most important example of the successful use of the 3D arrangement is the fin field-effect transistor (FinFET) [1].[1]

The channel length of a quantum analogue of the CMOS gate is determined by the capabilities of lithography. It was assumed in [3–6] that transport along the channel, which determines the transfer characteristic of the device, has a classical character, i.e., is described by the classical transport equations (drift–diffusion and kinetic equations), where quantum effects are taken into account in choosing the coefficients and parameters of classical models. The devices proposed in [3–6], where the switching between the logical levels occurs as a result of quantum mechanical tunneling relocation and transport has a classical character, can be classified as the first generation of the quantum analogues of CMOS gates.

Recent advances in nanoelectronics technology (and, first of all, in nanolithography) establish a realistic perspective for the appearance of semiconductor devices with characteristic feature dimensions (channel length) on the order of the electron wavelength [8]. Elements that small must be regarded as purely quantum objects (actually, molecules) whose distinction is the discreteness of the charge-carrier energy spectra. However, this statement is true only when the quantum object is isolated from the environment, while real devices always interact with the environment and therefore behave like open quantum systems, whose discrete energy levels transform into finite-width resonances. The transport of charge carriers in a quantum device is coherent and should be described in terms of the quantum mechanical transparency (electron-wave transmission coefficient), whose maxima correspond to resonances. The description of quantum mechanical transport is a complicated mathematical problem, but recent approaches [9–11] can offer a strategy to develop design principles for purely quantum devices. Such quantum devices implementing conventional Boolean functions may be called the second generation of the quantum analogues of CMOS gates.

This paper is organized as follows. In Section 2, we consider the mechanism of controlled relocation in the first-generation quantum analogues of CMOS gates and demonstrate that rapid dissipation-free relocation persists even in the presence of dissipative relaxation. In Section 3, we review the methods used for modeling coherent transport in open quantum systems on the basis of recent results on the behavior of interacting resonances in open quantum systems with exceptional points. In Section 4, we describe models of second-generation quantum analogues of CMOS gates, where charge-carrier transport is coherent. In the concluding part, Section 5, we discuss future prospects for the development of the quantum analogues of conventional logic gates implementing Boolean functions and place them in the context of the general development of quantum technologies.

[1] Field-effect transistor with a vertical channel resembling the fin of a fish.

2. First-generation quantum analogues of CMOS circuits: classical transport and quantum switching mechanism

2.1 Dissipationless relocation of the wave function in a quantum structure

The maximum of the electron density in a stationary state of a quantum structure with one occupied level in the absence of a periodic perturbation occurs at the lowest-energy level. In an asymmetric structure, the wave function corresponding to this level occupies one of the quantum wells. Under a slow adiabatic variation of an externally applied voltage, the system remains in the ground state at each moment of time [12], and the wave function undergoes slow relocation in space. In the opposite limit case of stepwise voltage switching, quantum mechanical calculations yield an oscillatory behavior for the probabilities of finding electrons in the two wells (quantum beats). In this case, relocation occurs via interwell intersubband relaxation assisted by the emission of phonons.

It was shown in [6] that in addition to the conventional dissipative mechanism of this switching, there is a dissipation-free mechanism of relocation under a two-step variation of voltage. In this case, relocation proceeds via a resonant state in which the wave function undergoes tunneling Rabi oscillations. Formally, this switching regime corresponds to a zero-reflection potential in a dynamic analogue of the stationary scattering problem for the Schrödinger equation; this potential can be specified explicitly for the two-level model [6]. Numerical simulations have demonstrated that dissipation-free relocation also occurs under a linear variation of the applied voltage with time, the characteristic duration of the switching process being of the order of the period of the tunneling Rabi oscillations. The time required to perform a logic operation is determined by the tunneling time and can be shorter than 1 ps [4].

This principle allows implementing quantum analogues of CMOS circuits that do not consume energy in the stationary state. Energy consumption in the transient regime can also be reduced considerably, which offers unique prospects for the fabrication of ultrahigh-speed circuits at the ultra-large-scale integration level. However, the approach used in [5, 6] to describe the dynamics of quantum CMOS circuits was based on solving the time-dependent Schrödinger equation, and therefore dissipation effects, which are inevitably present in real devices, were disregarded. In the next section, we use the density-matrix formalism to analyze the impact of dissipation effects on the controlled relocation of the electron density maximum in tunnel-coupled quantum wells.

2.2 Relocation of the wave function in a quantum structure with dissipation

The process of wave-function relocation can be illustrated in the simplest way with the example of a double-well heterostructure in an external electric field applied along the structure growth direction. Following [6], we consider a two-level system described by the Hamiltonian

$$\hat{H} = \begin{pmatrix} \varepsilon - \delta(t) & \tau \\ \tau & -\varepsilon + \delta(t) \end{pmatrix}. \tag{1}$$

where 2ε is the detuning between the quantum confinement energy levels in the two wells, τ is the tunneling matrix element, and $\delta(t)$ are the level shifts in the well owing to the applied external field. The time dependence of $\delta(t)$ determines the switching process in the device. At $t = 0$, the applied voltage is still zero and $\delta(0) = 0$. In this situation, the energy level in the left well is higher than the level in the right well, and the wave function is predominantly localized at the lower level (Fig. 2). After switching is complete, the voltage that sets in should correspond to the opposite picture, i.e., $\delta(t_0) = 2\varepsilon$, where t_0 is the duration of the switching process. Then, according to (1), the energy levels in the two wells are swapped and the lowest level appears in the left well, and hence the wave function predominantly relocates into that well.

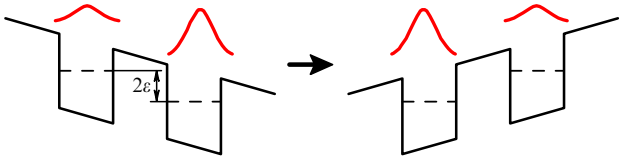

Figure 2. (Color online.) Relocation of the wave function in a double-well heterostructure. Red lines show the amplitudes of wave functions in the left and right wells of the structure.

Dissipative relaxation processes (which in this case are transitions from the upper to the lower level) can be properly taken into account by introducing the density matrix ρ of the system and describing its evolution using the Lindblad equation [13], which ensures that the positive definiteness of the density matrix is preserved and its trace equals unity [14]:

$$i\hbar \frac{\partial \rho}{\partial t} = [\hat{H}, \rho] + i\hbar \sum_k \Gamma_k \left(\hat{S}_k \rho \hat{S}_k^\dagger - \frac{1}{2} \hat{S}_k^\dagger \hat{S}_k \rho - \frac{1}{2} \rho \hat{S}_k^\dagger \hat{S}_k \right). \tag{2}$$

Here, $\hat{S}_k$ are the Lindblad operators describing the relaxation processes whose rates are characterized by the Γ_k. For the double-well system under consideration, which has two states with the energies $\varepsilon_L = \varepsilon - \delta(t)$ and $\varepsilon_R = -\varepsilon + \delta(t)$, localized in the left and right wells, relaxation transitions can occur both from the left to the right state and vice versa, depending on which of the two energies is higher. The Lindblad operators describing relaxation from the left to the right well and vice versa can be respectively chosen as

$$\hat{S}_1 = \begin{pmatrix} 0 & 0 \\ 1 & 0 \end{pmatrix},$$

and

$$\hat{S}_2 = \begin{pmatrix} 0 & 1 \\ 0 & 0 \end{pmatrix}.$$

The rate of relaxation, accompanied, for example, by the emission of optical phonons with an energy ε_{ph}, can be described by the quantities $\Gamma_1 = \Gamma\delta(\varepsilon_L - \varepsilon_R - \varepsilon_{ph})$ and $\Gamma_2 = \Gamma\delta(\varepsilon_R - \varepsilon_L - \varepsilon_{ph})$ for transitions from the left to the right well and vice versa (here, δ is the Dirac delta function).

As mentioned above, the rate of the relocation process depends on the shape of the control signal, i.e., the shape of the function $\delta(t)$. Because relaxation processes are slower than quantum mechanical oscillations, the optimum switching regime is obtained in the case of a two-

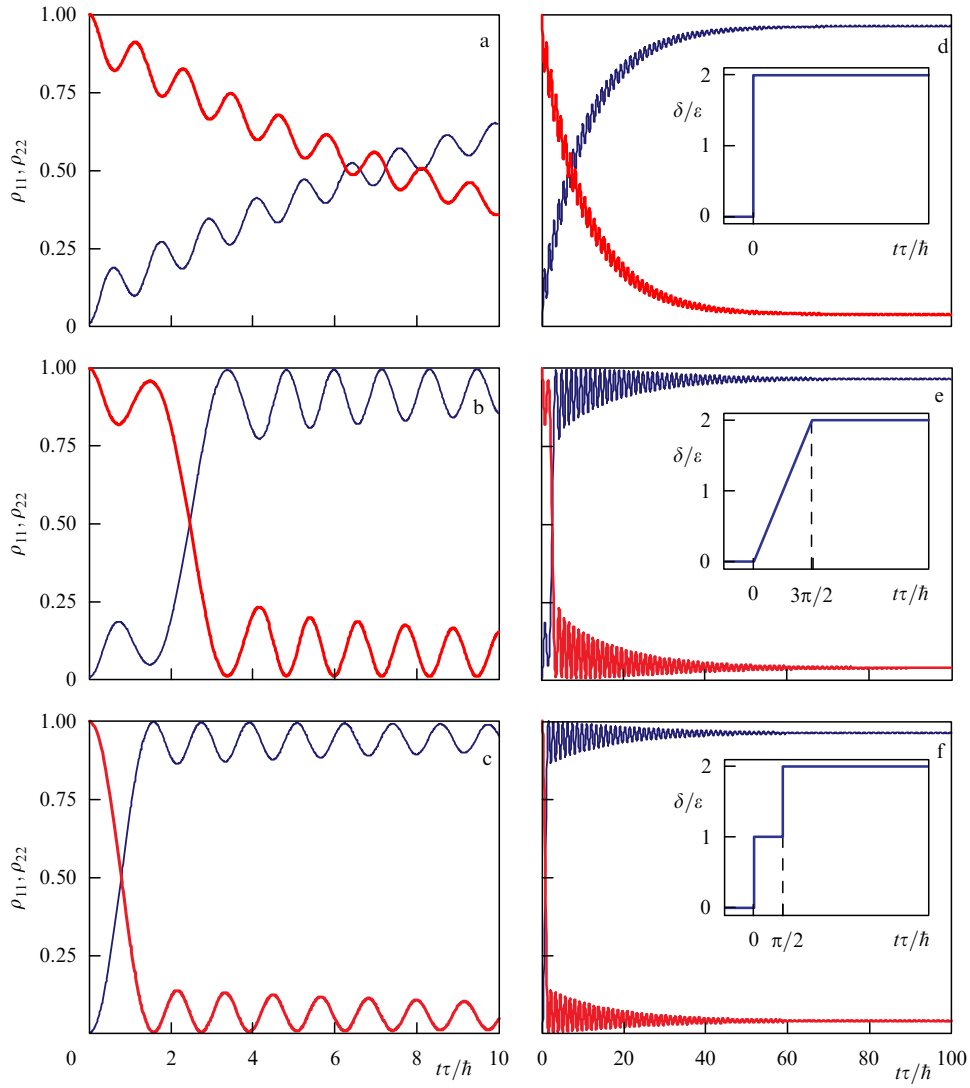

Figure 3. (Color online.) Evolution of the occupancies of the respective left and right quantum wells ρ_{11} and ρ_{22} (shown by respective thin blue and thick red lines), numerically calculated for the three switching regimes $\delta(t)$ depicted in the insets in panels (d)–(f). Panels (d)–(f) show the same occupancies as respective panels (a)–(c), but on a longer time scale. The parameters of the system are $\varepsilon = 2.5\tau$ and $\Gamma = 0.1\tau$.

step function $\delta(t)$ [6],

$$\delta(t) = \begin{cases} 0\,, & t < 0\,, \\ \varepsilon\,, & 0 \leqslant t < t_0\,, \\ 2\varepsilon\,, & t > t_0\,. \end{cases} \tag{3}$$

We can relate this function of time to a dynamic analog of the zero-reflection potential [6]. Figure 3 shows the occupancies of the left and right wells calculated numerically in accordance with Eqn (2) for different switching regimes, including the one specified by (3). It was assumed that the electron density is initially entirely localized in the right well:

$$\rho(0) = \begin{pmatrix} 0 & 0 \\ 0 & 1 \end{pmatrix}.$$

It can clearly be seen that under an abrupt single-step variation of the potential (Figs 3a, g), switching occurs only via the slower mechanisms of intersubband relaxation. Meanwhile, calculations of the time dynamics describing the relocation of the maximum of the wave-function amplitude in the occupied state demonstrate that the regime of rapid tunneling relocation under a two-step or linear variation of the voltage persists even when dissipation is taken into account. There are two time scales in these dynamics: one corresponds to rapid relocation and the other characterizes damping of the oscillations in the relocated wave function amplitude due to dissipation processes.

2.3 Implementation of the simplest logic circuits

The operation principle of the discussed quantum logic elements is based on the variation of the ohmic resistance of each quantum well with changes in the position of the peak of the squared absolute value of the wave function of the system. Figure 1b shows the basic layout of a double-well quantum inverter. The power supply voltage V_0 is applied between the terminals that are individually connected to wells 1 and 2, and the input voltage V_{in} is applied to the top gate (control electrode), separated from the upper well by a wide tunneling-opaque barrier. The output voltage V_{out} is read off from the common terminal contacting both wells. When the maximum of the electron density is in the first quantum well, its lateral resistance is much lower than that of the second well. When the control voltage is applied to the top gate of the structure, the supply current flows along the other

well, and the output signal of the inverter changes from the logic 0 to the logic 1 voltage.

In contrast to its classical prototype, this quantum analogue of the CMOS circuit has a functionally integrated structure, in which the control electrode (input) is placed on the top surface of the heterostructure with two potential wells separated by a tunneling-transparent barrier. A feature of the functionally integrated structure is the requirement of individual ohmic contacts with each potential well (the power supply bus and the output contacts). Apart from the main benefit of classical CMOS circuits (the absence of the current in the stationary state), this design solution offers a number of additional advantages. One of them is the possibility of a considerable reduction in the through currents in the transient regimes in multiple-well quantum elements (three or more wells) [3–5]. This is an essential advantage that allows eliminating one of the main contributions to power consumption, whose importance increases with increasing the switching rate. Similarly to the classical CMOS elements, current in the power supply bus of their quantum analogues flows only during a switching transient, i.e., during the relocation of the wave function maximum between the wells. Another important advantage of the suggested design is its high-density structural and topological implementation at the level of multiple-input NAND and NOR logic gates with no metallized interconnects between circuits (Fig. 4).

Changing the configuration of wave functions in the quantum wells by a transverse electric field requires that the potential drop in the region of the wells be of the order of the energy difference between the quantum confinement levels. When the control voltage is applied between the source and the gate, the electric field is screened by charge carriers in the quantum well that is closer to the gate. Therefore, in order to create a transverse electric field, the quantum wells are placed between two gates (the top and bottom ones). The fabrication of a bottom gate with low leakage currents and of separate contacts with the two gate electrodes is a challenging technological problem. For example, in [15] this problem was solved by introducing a high-resistivity region beneath the ohmic contacts with the quantum wells, which was attained by irradiation with gallium ions. This technology is too complicated, costly, and insufficiently reliable. Furthermore, the presence of two control electrodes is inconvenient from the practical standpoint.

A transistor structure with tunnel-coupled quantum wells that can be efficiently controlled by only one (the top) gate electrode was proposed in [16]. In this transistor, the conducting channel is formed by two undoped GaAs quantum wells of significantly different thicknesses separated by a tunneling-transparent $Al_{0.3}Ga_{0.7}As$ barrier with a thickness of about 100 Å. The growth conditions for the quantum well located closer to the gate were chosen such that the charge-carrier mobility in this well decreased to ~ 100 cm^2 (V s)$^{-1}$. Because the conductivity of such a quantum well is nearly absent, it does not screen the electric field of the gate electrode in the region of the second well, and the structure is efficiently controlled by just the top gate. The mobilities in the two quantum wells differ by about two orders of magnitude. A change in the voltage applied to the gate electrode leads to the relocation of the electron wave function between the wells, and the channel conductivity changes owing to the large difference between the carrier mobilities.

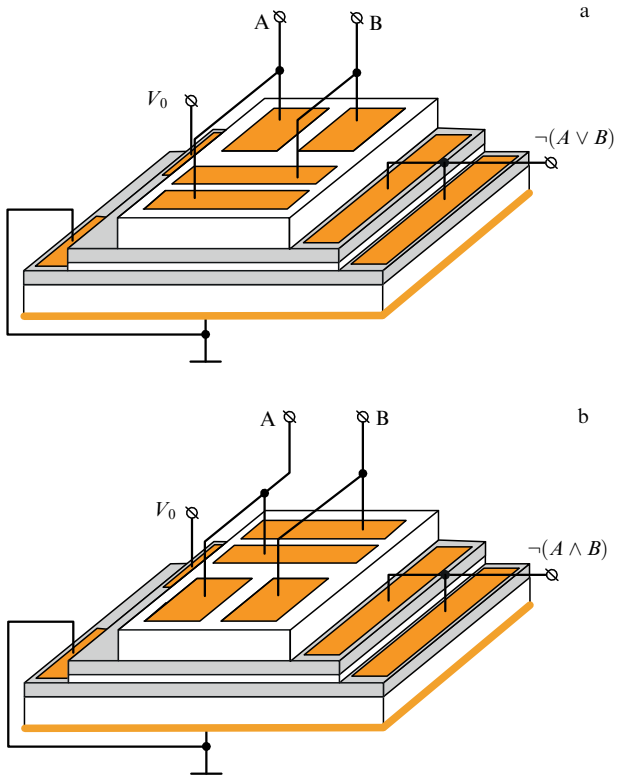

Figure 4. (Color online.) Layouts of (a) NOR and (b) NAND quantum logic elements. Contact pads and GaAs quantum wells are respectively shown in orange and gray.

Consistently implementing the principle of local readout of data from the quantum wells of the structure under applying a control voltage to the gate allows synthesizing a functionally complete set of logic elements of a new type [4, 5]. The devices can feature parallel (along the potential well from the power supply bus contact to the output terminal) or perpendicular input electrodes. Each of these electrodes induces the wave function relocation only over some part of the quantum-well layer, i.e., locally. As a result, multiple-input NAND (Fig. 4a) or NOR (Fig. 4b) elements are produced. The proposed design is based on the fact that the maximum of the wave function amplitude squared relocates locally. This means that relocation occurs only within the part of the quantum structure beneath the control electrode of the device, formed on the top of the tunneling-opaque barrier.

Despite a number of advantages, the quantum analogues of CMOS gates have not been put into practice because of technological difficulties in making local contacts to the quantum wells. Currently, this technology is receiving fresh impetus for development in view of the fabrication of 3D memory devices. This may also offer new prospects for the implementation of the quantum analogues of CMOS circuits considered in this section.

3. Quantum transport and resonances: a unified theory of resonances and antiresonances

3.1 Open quantum systems and resonances

In the quantum analogues of CMOS gates described in the preceding section, switching from one state to another (i.e., switching between the logic levels of the device) occurs as a

result of coherent quantum mechanical evolution in tunnel-coupled quantum wells. Meanwhile, the formation of the logic levels themselves, which correspond to certain voltages at the output of the device, occurs via the process of classical charge-carrier transport along the quantum wells. With a decrease in lateral dimensions (i.e., actually, upon the transition to molecular structures with a discrete energy spectrum), charge transport through the device occurs quantum mechanically. However, information is still input to the device and output from the device by setting and reading certain values of voltage, i.e., in the classical form. The need for an interface providing a link to the classical environment is an inherent feature of any quantum device, including quantum computers [17, 18]. In fact, any quantum system is an open system, because it interacts with a measuring device and the environment.

The properties of open quantum systems and the techniques used to describe them differ essentially from those of closed quantum systems. The main difference is that in contrast to closed quantum systems, an open quantum system has no stationary states, because any state acquires a finite lifetime. Formally, the absence of stationary states in open quantum systems can be represented by introducing complex energies whose real and imaginary parts respectively correspond to the energy proper of a particle at a given level and to the width ΔE of that level (which, according to Heisenberg's uncertainty principle $\Delta E \Delta t \geqslant \hbar/2$ is related to the uncertainty in the particle lifetime in this state, Δt), determined by the average outgoing momentum flux [19].

We note that all observables (including energy) characterizing the full system consisting of both the quantum system under consideration and its environment remain real. Complex energy values and non-Hermitian operators appear in passing to a reduced description dealing only with the quantum system itself, albeit taking its openness into account. This is realized most clearly in Feshbach's papers [20–22], where the concept of the non-Hermitian Hamiltonian of an open quantum system was introduced. In contrast to closed quantum systems, the behavior of open quantum systems is described by non-Hermitian operators, which brings about fundamentally new properties.

The eigenstates of an open quantum system can also be defined as solutions of the Schrödinger equation with boundary conditions requiring the existence of only outgoing waves [23]. These states, called resonance states, can be classified according to the signs of the imaginary part of the energy and the wave vector of the outgoing wave (see, e.g., [19, 24]). The interaction of an open quantum system with its environment was described in detail by Fano [25].

If the widths of resonance states (determined from their lifetimes) are much smaller than the difference between the energies of neighboring states, particle escape from these states is exponential and occurs independently for each state, and hence the probability of finding the particle in such a state is $P \propto \exp(-\Gamma t)$, where $\Gamma = \hbar/\tau$ is the level width and τ is its lifetime. However, when the energy spacing between resonance levels becomes comparable to their widths, the influence of the resonance levels on each other has to be taken into account and can lead to various nontrivial effects. Thus, it was shown in [26] that as the interaction of an open quantum system with its environment becomes stronger, only part of its levels broaden correspondingly, and the number of levels whose width increases is equal to the number of channels for particle escape from the system. The Fano approach was extended to the case of overlapping resonances in [27]. Especially noteworthy is the 'level repulsion' effect [28, 29]: the complex energies of resonance states do not coincide in the complex plane as the system parameters are varied. In particular, under an increase in the strength of the interaction of an open quantum system with its environment, some levels can have the same real part of the energy but different imaginary parts. This leads to a nontrivial behavior manifesting itself in the occurrence of long-lived levels, in addition to short-lived ones, as the interaction of an open quantum system with its environment becomes stronger (see, e.g., [30]), which was confirmed experimentally, in particular, for an open microwave cavity [31].

Resonance scattering plays an important role in the physics of open quantum systems and optical waveguides [32–34]. For this reason, the capability to create nanoelectronic and nanophotonic structures with the desired resonance properties is of primary importance. Recently, there has been steady progress in understanding open quantum systems, as well as open microwave and optical systems [32–35].

Traditionally, the scattering problem for nanoscale systems is described in terms of the scattering matrix (the S-matrix) [12]. The scattering matrix relates the amplitudes of waves incident on the system (the scattering center) with the amplitudes of scattered waves. States where outgoing waves exist in the absence of incoming waves are special in this theory; these states correspond to the scattering matrix poles and represent nothing more than resonance states in Siegert's formulation [23]. Therefore, the poles of the scattering matrix correspond to eigenvalues of the effective Hamiltonian of the scattering system. However, the energies corresponding to the scattering matrix poles are complex, while actual processes occur only for real energies of the scattered particles. It is therefore important to properly relate the properties of the system with real energies to the analytic properties of its scattering matrix.

In the traditional approach to the physical interpretation of the complex energies of resonance states in the scattering problem [36], the scattering cross section (or the transmission amplitude in the one-dimensional case) has a symmetric maximum positioned at the energy equal to the real part of the complex resonance energy and having a half-width equal to its imaginary part (Breit–Wigner resonance). In the one-dimensional case, the corresponding transmission probability is

$$T_{\mathrm{BW}}(E) = \frac{4\Gamma_1\Gamma_2}{(\Gamma_1+\Gamma_2)^2 + (E-E_0)^2}\,, \tag{4}$$

where E_0 is the resonance position (real part) and $\Gamma_1 + \Gamma_2$ is the resonance half-width (imaginary part), which is determined by the strength of coupling to the continuum of states to the left and to the right of the scattering system (Γ_1 and Γ_2, respectively). However, this interpretation is correct only in the case of narrow, well-separated maxima, when the imaginary parts of the corresponding poles are small in comparison to the difference between their real parts. Resonance maxima can coalesce as they approach each other and broaden, although the scattering matrix poles may still have different real parts. Therefore, the correspondence between the poles and the resonance maxima is not one

to one in general. It was shown in [37] that in the case of broad but still isolated resonances, the position of the maximum is estimated better as the absolute value of the pole rather than its real part.

The coalescence of resonances that cannot be described in terms of scattering-matrix poles seems to have been considered for the first time in [38] in the example of a one-dimensional symmetric triple-barrier structure. Later, the coalescence of three unit resonances in a system of quantum dots was discussed in [29]. The results of numerical simulations that give evidence of the coalescence of two resonances were presented in book [39]. The coalescence (collapse) of two unit resonances accompanied by the formation of one resonance with a transparency smaller than unity in the cases of a triple barrier, an inverted double barrier, and some other symmetric structures was analyzed in [40], where it was regarded as a quantum phase transition. Importantly, the transparency of the system in the regime of resonance coalescence differs considerably from the Breit–Wigner shape:

$$T_{\text{coalescence}}(E) = \frac{4\Gamma^{2N}}{4\Gamma^{2N} + (E - E_0)^{2N}}\,, \tag{5}$$

where $\Gamma = \Gamma_1 = \Gamma_2$ is the tunneling coupling with the leads in a symmetric structure and N is the number of coalescing resonances (in [40], $N = 2$). It was also shown in [40] that the coalescence of resonances in a symmetric structure is accompanied by a symmetry breaking of the electron density distribution. This breaking occurs abruptly, and the asymmetry parameter behaves like an order parameter in a quantum phase transition.

The scattering matrix poles (eigenvalues of the effective Hamiltonian) can also coalesce with the formation of second- and higher-order poles [41–43]. However, generally, this has no direct relation to the coalescence of resonances and hence to the properties of observables. Nevertheless, the physical properties of the system change as the eigenvalues of the S-matrix merge (they cease to be unimodular), which is possible, e.g., in systems with balanced losses and amplification [44, 45].

In a quantum system where a charge carrier can travel along different trajectories (tunneling paths), interference between them is possible. One typical example of this interference is the Aharonov–Bohm effect [46]. Fano showed in 1961 that in the case of the scattering of a particle on a system with a bound state, the profile of the scattering cross section (transmission coefficient in the one-dimensional case) can be asymmetric [25]. This is due to the possible destructive interference of waves passing via the bound state of the system and 'bypassing' this state. Subsequently, it was established that the Fano resonance is a universal phenomenon that can occur in a variety of physical systems [33].

3.2 Exceptional points in open quantum systems and *PT* symmetry

Traditionally, observables are represented in quantum mechanics by Hermitian operators, which ensures that their eigenvalues are real [12]. Energy and the corresponding operator (the Hamiltonian) stand out among other observables. The fact that energy is real and the Hamiltonian is Hermitian ensures the unitary evolution of the wave function, i.e., the conservation of its norm (the number of particles). However, it turns out that certain classes of non-Hermitian operators can also have real eigenvalues. In 1998, Bender and Boettcher analyzed the spectrum of non-Hermitian Hamiltonians that have symmetry under the simultaneous inversion of coordinates (P) and time (T), but have no symmetry under each inversion separately. It was shown by numerical methods that entirely real energy spectra can appear in systems with PT-symmetric non-Hermitian Hamiltonians. Later, Bender, Boettcher, and Meisinger demonstrated that traditional quantum mechanics can be extended to the case of PT-symmetric non-Hermitian systems [48]. The problem of the possible nonunitary evolution of a system described by a PT-symmetric non-Hermitian Hamiltonian was also solved in [49]. We note that soon after the discovery that PT-symmetric Hamiltonians have a real spectrum, it was established that the necessary condition for the real-valuedness of the spectrum of a Hamiltonian is its pseudo-Hermiticity, of which PT symmetry is only a particular case [50–52]. However, PT-symmetric systems still deserve to be singled out because they play a special role in optics [53].

A key feature of PT-symmetric operators is the phenomenon of spontaneous PT symmetry breaking accompanied by the violation of the realness of the eigenvalues. This occurs under varying some tuning parameter characterizing the system. Under this transformation, real eigenvalues coalesce and then become complex. This occurs pairwise [54, 55]: a pair of real eigenvalues coalesce and, with a further variation of the tuning parameter, transform into a pair of complex-conjugate eigenvalues. At the value of the tuning parameter where two real eigenvalues of the operator coincide, the spectrum is degenerate. However, this degeneracy is fundamentally different from that in the case of Hermitian operators. A Hermitian operator can always be diagonalized and has orthogonal eigenvectors at the degeneracy point. For example, the Hamiltonian of a two-level system describing degenerate states has the form

$$\hat{H}_{\text{DP}} = \begin{pmatrix} E_0 & 0 \\ 0 & E_0 \end{pmatrix}. \tag{6}$$

A point in the parameter space where such a degeneracy of the system occurs is called a diabolic point. PT-symmetric operators turn out to be nondiagonalizable at the degeneracy point because, in addition to eigenvalues, eigenvectors also coalesce. In the case of a two-level system, the Hamiltonian then assumes the form

$$\hat{H}_{\text{EP}} = \begin{pmatrix} E_0 & A \\ 0 & E_0 \end{pmatrix}, \tag{7}$$

where $A \neq 0$. A point in the parameter space corresponding to this degeneracy mechanism is called an exceptional point [56]. Exceptional points attract much interest in relation to the nonanalytic behavior of the operator eigenvalues in their vicinity.

Because the Hamiltonian of any closed system is a Hermitian operator, only an open quantum system can have a non-Hermitian, in particular, PT-symmetric, Hamiltonian. Owing to the possibility of nonunitary evolution (i.e., evolution where particle number conservation is violated) in a PT-symmetric system, it is unclear whether such a system can be implemented for fermions (although it should be mentioned that bound states related to an exceptional point can appear for exotic Majorana fermions [57, 58]). For bosons, the implementation of a PT-symmetric system is a

more tractable problem because PT symmetry can be realized as a mirror-symmetric distribution of regions where bosons are created and annihilated. A PT-symmetric Bose–Einstein condensate has been considered, e.g., in [59]. Another example of bosonic systems is given by superconductors, where PT symmetry breaking was observed experimentally in the spectrum of fluctuations [60].

Because the wave equation describing the propagation of electromagnetic waves is mathematically equivalent to the quantum mechanical Schrödinger equation, PT-symmetric systems can also be implemented in optical structures [61]. In this case, the imaginary terms in the dielectric function describe well-defined processes of signal absorption and amplification. Currently, effects related to PT symmetry and its breaking are primarily investigated for various optical structures. The PT-symmetric systems under consideration are quite diverse: photonic crystals [62], microwave cavities [63], PT-symmetric plasmonic metamaterials [64, 65], lasers [66], etc. The occurrence of an exceptional point in PT-symmetric systems changes many of their properties qualitatively. For example, the transparency of the system can increase with increasing absorption [61] or the intensity of laser radiation can decrease with increasing the pump power [67]. We note, however, that optical systems are subject to a fundamental limitation, which is absent in quantum mechanics and which implies that the dielectric function of a medium cannot be arbitrary. Indeed, any response function (in particular, the dielectric function) must satisfy the causality principle and therefore the Kramers–Kronig relations [68]. For this reason, the dielectric function has to have dispersion if its imaginary part is nonzero, and then the PT symmetry condition can be satisfied only for a discrete set of frequencies [69].

The relation between the perfect transparency of a quantum system and the asymptotic PT symmetry of the effective Hamiltonian was discussed in [70]. However, the idea of a correspondence between a resonance state (i.e., a state with unit transparency) in a Hermitian problem and a certain auxiliary PT-symmetric scattering problem was put forward in [71, 72]. The same authors subsequently extended their result and demonstrated that the scattering problem in an arbitrary open Hermitian system with two contacts can be reformulated as a scattering problem for a certain non-Hermitian Hamiltonian [72].

The idea about the relation between the resonance states of a Hermitian problem and an auxiliary PT-symmetric Hamiltonian was recently used in [9, 10] to describe the coalescence of an arbitrary (even) number of resonances in a symmetric multiple-barrier structure with an arbitrary (odd) number of barriers as a transition with PT symmetry breaking in the auxiliary Hamiltonian. A similar idea was put forward in [73], where the coalescence of two unit resonances was described as the PT symmetry breaking in a certain auxiliary Schrödinger equation for the envelope wave function with the Robin boundary condition. It was shown in [9, 10] that the exact positions of the unit transmission maxima is determined by the real eigenvalues of the additional PT-symmetric Hamiltonian, and hence the coalescence of resonances represents the breaking of PT symmetry of the auxiliary Hamiltonian and the transition from real to complex eigenvalues. At the coalescence point itself, the energy dependence of transparency is described by a non-Breit–Wigner expression in Eqn (5); with an increase in the number of coalescing resonances, its shape approaches that of the transmission coefficient of a band-pass filter.

In the general case of an arbitrary quantum system confined between two contacts, the tunneling transparency is determined by the usual expression [74]

$$T = \mathrm{Tr}\,(\Gamma_{\mathrm{L}} G^{\mathrm{r}} \Gamma_{\mathrm{R}} G^{\mathrm{a}})\,, \tag{8}$$

where Γ_{L} and Γ_{R} are the imaginary parts of the self-energy corrections caused by the interaction with contacts, and G^{r} and G^{a} are the retarded and advanced Green's functions of the system (taking contacts into account). After the calculation of the Green's functions, Eqn (8) yields an expression for transparency in terms of the Feshbach effective Hamiltonian $\hat{H}_{\mathrm{eff}}$ [20–22]:

$$T = \frac{4\sum_{i,j,m,k=1}^{N} (-1)^{i+j+m+k} M_{ij}^{*} M_{mk} \Gamma_{jk}^{\mathrm{R}} \Gamma_{mi}^{\mathrm{L}}}{\left|\det\left(E\hat{I} - \hat{H}_{\mathrm{eff}}\right)\right|^{2}}\,. \tag{9}$$

Here, M_{ij} are the corresponding minors of the matrix $E\hat{I} - \hat{H}_{\mathrm{eff}}$. According to [11], Eqn (8) and hence Eqn (9) can be rewritten such that they depend only on the characteristic determinants of the Feshbach effective Hamiltonian and another non-Hermitian Hamiltonian $\hat{H}_{\mathrm{aux}}$, which can be obtained directly from the effective Hamiltonian:

$$T = \frac{|E\hat{I} - \hat{H}_{\mathrm{eff}}|^{2} - |E\hat{I} - \hat{H}_{\mathrm{aux}}|^{2}}{|E\hat{I} - \hat{H}_{\mathrm{eff}}|^{2}}\,, \tag{10}$$

or, in a more compact form,

$$T = \frac{|P|^{2}}{|P|^{2} + |Q|^{2}}\,, \tag{11}$$

where P and Q are functions of energy in general; Q is the characteristic determinant of the auxiliary non-Hermitian Hamiltonian:

$$Q = \det\left(E\hat{I} - \hat{H}_{\mathrm{aux}}\right). \tag{12}$$

For a simply connected system, P is a constant, and Eqn (11) for a single site (a system with a single energy level) becomes the Breit–Wigner formula. For a multiply connected system, P becomes a function of energy. According to Eqn (11), the exact positions of zeros and of unity transmission maxima are determined as real zeros (roots) of the respective functions P and Q. For a spatially symmetric system, the auxiliary Hamiltonian becomes PT symmetric and can have exceptional points where two real roots characterizing unit resonances coalesce and transform into a pair of complex-conjugate ones, which determines a single non-unit resonance. Using this approach, in particular, allows describing a structure consisting of two identical symmetric linear chains of sites where transmission zeros coalesce with the formation of a broad reflection window. In this case, the transmission coefficient has the form

$$T(E) = \frac{(E - E_0)^{2N}}{(E - E_0)^{2N} + \Gamma^{2N}}\,. \tag{13}$$

It has been demonstrated that a structure with either a broad transparency or broad opacity window can be obtained on the basis of the same symmetric linear chain. In fact, the

results in [9–11] offer a unified theory of resonances and antiresonances (Fano–Feshbach resonances), which can be described by the general formula (11). We note that the case where P and Q vanish simultaneously corresponds to a bound state in the continuum; such states have been actively investigated in recent years in condensed matter physics and optics [35].

4. Second-generation quantum analogues of CMOS circuits: molecular structures with controllable resonances

4.1 General operation principles of a quantum inverter

We consider a model structure of a quantum inverter (Fig. 5), similar to the structure of a classical CMOS inverter (Fig. 1a), with the complementary MOS transistors replaced with two quantum systems that do not interact with each other and have the Hamiltonians $\hat{H}_1$ and $\hat{H}_2$. These quantum systems (for example, molecules) play the role of switches controlled by the electric field of a control electrode (gate) ('quantum transistors'). Both systems are tunnel-coupled to the output contact and to contacts to which reference voltages V_{ref1} and V_{ref2} are applied (these are typically determined by the common-bus ('ground') potential and the power supply voltage). The input voltage is applied to the contact that is only electrostatically coupled to the quantum systems and affects them only via the electric field (potential), i.e., with no charge-carrier transfer. Each quantum system in this structure is a quantum conductor, whose transport properties cannot be described by the classical drift–diffusion model, as was the case with the first-generation quantum analogues of CMOS gates considered in Section 2.

The current flowing through a quantum conductor under the conditions of ballistic transport can be calculated using the well-known expression [74]

$$I = \frac{e}{h}\int_{-\infty}^{\infty} T(E)\big(f_{\mathrm{L}}(E) - f_{\mathrm{R}}(E)\big)\,\mathrm{d}E, \tag{14}$$

where $T(E)$ is the transmission coefficient of the quantum system, determined by Eqn (11). The difference between the Fermi–Dirac distribution functions f_{L} and f_{R} in the left and right contacts determines the effective range of integration in the above expression.

If the transmission coefficients of the quantum systems are known, we can use Eqn (14) to calculate currents flowing through all output contacts in the inverter structure shown in Fig. 5:

$$\begin{aligned}
I_{\mathrm{ref1}} &= \frac{e}{h}\int\Big[T_{1\mathrm{out}}(E)\big(f(E-eV_{\mathrm{ref1}}) - f(E-eV_{\mathrm{out}})\big) \\
&\quad + T_{12}(E)\big(f(E-eV_{\mathrm{ref1}}) - f(E-eV_{\mathrm{ref2}})\big)\Big]\,\mathrm{d}E, \\
I_{\mathrm{ref2}} &= \frac{e}{h}\int\Big[T_{2\mathrm{out}}(E)\big(f(E-eV_{\mathrm{ref2}}) - f(E-eV_{\mathrm{out}})\big) \\
&\quad + T_{12}(E)\big(f(E-eV_{\mathrm{ref2}}) - f(E-eV_{\mathrm{ref1}})\big)\Big]\,\mathrm{d}E, \\
I_{\mathrm{out}} &= \frac{e}{h}\int\Big[T_{1\mathrm{out}}(E)\big(f(E-eV_{\mathrm{out}}) - f(E-eV_{\mathrm{ref1}})\big) \\
&\quad + T_{2\mathrm{out}}(E)\big(f(E-eV_{\mathrm{out}}) - f(E-eV_{\mathrm{ref2}})\big)\Big]\,\mathrm{d}E.
\end{aligned} \tag{15}$$

These expressions are in fact an example of Büttiker's multiterminal formalism [75] for finite voltages. Here, $T_{1\mathrm{out}}$, $T_{2\mathrm{out}}$, and T_{12} are the probabilities of tunneling between the corresponding contacts. Assuming that the systems do not interact with each other, we can set $T_{12} = T_{1\mathrm{out}}T_{2\mathrm{out}}$. The reference voltages V_{ref1} and V_{ref2} (assuming that $V_{\mathrm{ref1}} < V_{\mathrm{ref2}}$) are determined by ideal external sources and are assumed to be constant hereafter. The input contact is galvanically isolated from the rest of the system and affects only the transmission coefficients owing to the shift of the energy levels in the two quantum systems in an electric field.

The principle of operation of a quantum inverter (see Fig. 5) is similar to that of a classical CMOS inverter (Fig. 1a) described in the Introduction. If a high-resistance load (e.g., the input of the next inverter or another logic gate) is connected to the output contact of a quantum inverter, the current running through this contact is zero ($I_{\mathrm{out}} = 0$). We assume that for a given applied voltage, the transparency of the first quantum system is very low ($T_{1\mathrm{out}} \approx 0$), for example, because resonances are shifted away from the effective integration region. Then the first term in the integrand in expression (15) for the output current vanishes, and the condition $I_{\mathrm{out}} = 0$ implies that the second term must also vanish. Under the assumption that the transparency $T_{2\mathrm{out}}$ is nonzero, the output current can vanish only when $V_{\mathrm{out}} \approx V_{\mathrm{ref2}}$. It can easily be seen from Eqn (15) that under the conditions $T_{1\mathrm{out}} \approx 0$ and $V_{\mathrm{out}} \approx V_{\mathrm{ref2}}$, the currents I_{ref1} and I_{ref2} must also vanish. The same situation occurs for the other input voltage, which ensures that $T_{2\mathrm{out}} \approx 0$. Then the condition $I_{\mathrm{out}} = 0$ implies that $V_{\mathrm{out}} \approx V_{\mathrm{ref1}}$, while the currents I_{ref1} and I_{ref2} again vanish. For self-consistency, the parameters of the system should be chosen such that the transparencies are low: $T_{1\mathrm{out}} \approx 0$ for $V_{\mathrm{in}} \approx V_{\mathrm{ref1}}$ and $T_{2\mathrm{out}} \approx 0$ for $V_{\mathrm{in}} \approx V_{\mathrm{ref2}}$. The absence of currents and hence of power consumption in the stationary state is the main advantage of CMOS circuits, which consume power only in the process of switching. The consumed power is proportional to the square of the supply voltage $V_0 = V_{\mathrm{ref1}} - V_{\mathrm{ref2}}$ and inversely proportional to the switching time [76].

Thus, in order to attain an increase in speed, it is necessary, in addition to decreasing characteristic dimensions, to reduce power consumption. However, in spite of considerable advances in scaling down nanoelectronic elements, the supply voltage of modern CMOS gates still cannot be made much lower than 1 V [76]. This stimulates the search for new device solutions. One of them is tunnel transistors with band-to-band tunneling, operating under a supply voltage V_0 below 0.5 V [77]. We can accordingly estimate the upper limit for the practically interesting range of supply voltages for future molecular quantum gates at 0.1–0.2 V.

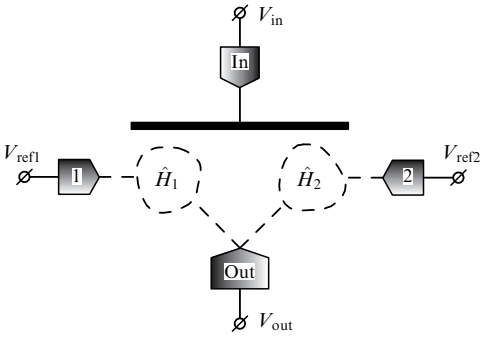

Figure 5. Schematic of a quantum analogue of the CMOS inverter.

4.2 Manipulating resonances in a quantum inverter

Switching in molecular quantum gates relies on controlling resonances in the quantum structures forming the gate. We first consider a quantum gate where switching between the logic levels is physically implemented by a controlled shift of the resonances. Let the transmission coefficients $T_{1\mathrm{out}}$ and $T_{2\mathrm{out}}$ have narrow peaks at the respective energies $E = E_1$ and $E = E_2$, on some constant background $T_\mathrm{b} \ll 1$ originating from other resonances remote in energy:

$$T_{1,2\mathrm{out}} = T_\mathrm{b} + A\,\frac{4\Gamma^2}{4\Gamma^2 + (E - E_{1,2})^2}\,, \tag{16}$$

where $\Gamma/(k_\mathrm{B}T) \ll 1$ (k_B is the Boltzmann constant). In this phenomenological expression, the parameter Γ determines the strength of interaction between the system and the continuum of states in the contacts and, thus, the resonance width (the effects of population trapping [30, 31] and resonance narrowing [27, 78, 79] are beyond the scope of this model); the parameter $0 \leqslant A \leqslant 1 - T_\mathrm{b} \approx 1$ determines the resonance height. For example, in the case of asymmetric tunneling couplings to the left and right contacts Γ_L and Γ_R, the value of Γ in Eqn (16) is simply the half-sum $\Gamma = (\Gamma_\mathrm{L} + \Gamma_\mathrm{R})/2$, and the resonance height is determined by the coefficient $A = \Gamma_\mathrm{L}\Gamma_\mathrm{R}/\Gamma^2$. The parameter T_b is the 'background' transparency describing contributions to the transmission coefficient from states that are far away from the resonance level under consideration. First-principle calculations indicate that $T_\mathrm{b} = 10^{-1} - 10^{-3}$ in real molecular structures (see, e.g., [80–82].) This value determines the stationary-state current (leakage) through the gate.

Taking into account that the second term in expressions (16) for $T_{1\mathrm{out}}$ and $T_{2\mathrm{out}}$ differs from zero only in a range of energies around E_1 or E_2, which is much narrower than the effective integration range, the condition $I_\mathrm{out} = 0$, which determines the output voltage, can be written as

$$f(E_1 - eV_\mathrm{out}) - f(E_1 - eV_\mathrm{ref1}) + \frac{T_\mathrm{b}e}{2\pi\Gamma A}(V_\mathrm{out} - V_\mathrm{ref1})$$
$$\approx f(E_2 - eV_\mathrm{ref2}) - f(E_2 - eV_\mathrm{out}) + \frac{T_\mathrm{b}e}{2\pi\Gamma A}(V_\mathrm{ref2} - V_\mathrm{out})\,. \tag{17}$$

To obtain a symmetric transfer characteristic, it is necessary to choose the reference voltages V_ref1 and V_ref2 such that for the input voltage $V_\mathrm{in}^0 = (V_\mathrm{ref1} + V_\mathrm{ref2})/2$, the resonances be arranged symmetrically with respect to eV_in^0. Taking the effect of the input potential into account, we can formulate the conditions

$$\frac{1}{2}(E_1 + E_2) = eV_\mathrm{in}^0 + e\alpha(V_\mathrm{in} - V_\mathrm{in}^0)\,,$$
$$E_2 - E_1 = e(V_\mathrm{ref2} - V_\mathrm{ref1}) + 2ck_\mathrm{B}T\,. \tag{18}$$

Here, $0 < \alpha < 1$ determines the electrostatic coupling relation between the input control potential (measured with respect to V_in^0) and the positions of the energy levels in the quantum systems, and c is the difference between the resonance positions (in units of $2k_\mathrm{B}T$) with respect to the difference in the reference voltages. The value of α depends considerably on the thickness of the insulator layer separating the control electrode [83]; its typical values are of the order of 0.1 or smaller [84], but, theoretically, it can be as high as 0.5–0.7 for insulator thicknesses of about 1 nm [83]. The possibility of obtaining $\alpha \sim 0.2-0.3$ was demonstrated experimentally in [85, 86]. Figure 6 schematically shows the transparency of the quantum systems and the corresponding difference in the distribution functions for input voltages corresponding to the logic 0 and logic 1. Disregarding the background contribution to the transparency, condition (17) can be illustratively represented as the requirement that the differences between the corresponding distribution functions calculated at the energies of the resonance peaks coincide.

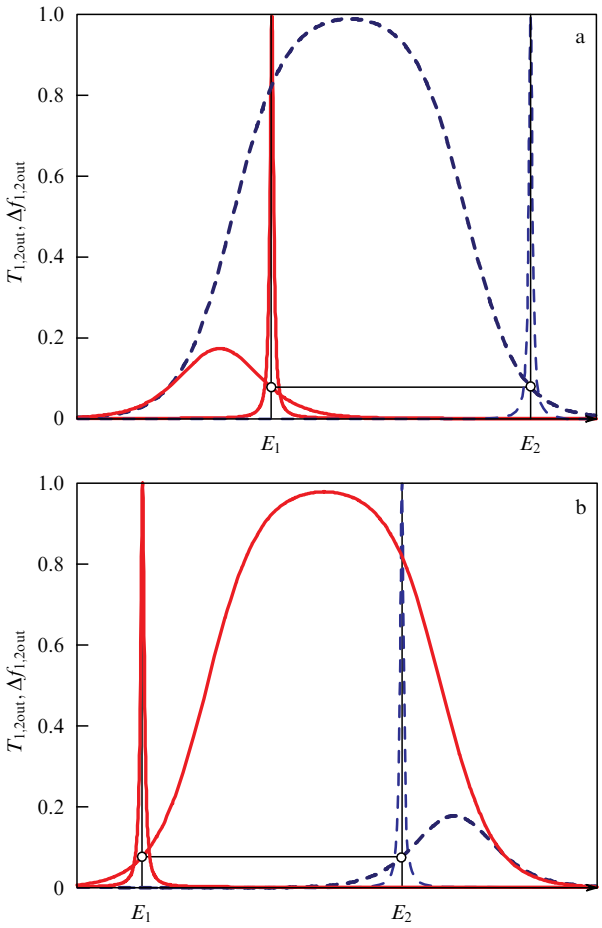

Figure 6. (Color online.) Plots illustrating condition (17), from which the output voltage of an inverter controlled by the shift of transmission resonances is determined. The two panels correspond to the input voltages of (a) the logic 1 ($V_\mathrm{in} = V_\mathrm{ref2}$) and (b) logic 0 ($V_\mathrm{in} = V_\mathrm{ref1}$). Thin lines show the transmission coefficients $T_{1\mathrm{out}}$ and $T_{2\mathrm{out}}$ calculated disregarding the 'background' contribution (solid red and dashed blue lines, respectively); thick lines show the differences in the distribution functions $\Delta f_{1\mathrm{out}} = f_\mathrm{out} - f_1$ and $\Delta f_{2\mathrm{out}} = f_2 - f_\mathrm{out}$ (solid red and dashed blue lines, respectively). If the 'background' transparency is disregarded, condition (17) reduces to the requirement $\Delta f_{1\mathrm{out}}(E_1) = \Delta f_{2\mathrm{out}}(E_2)$.

Substituting relations (18) in Eqn (17), we can determine the output voltage $V_\mathrm{out} = V_\mathrm{out}(V_\mathrm{in})$ as a function of the input voltage and analytically estimate the main parameter of the transfer characteristic, i.e., the highest absolute value of the gain coefficient $g = |\partial V_\mathrm{out}/\partial V_\mathrm{in}|$, which, because of the symmetry, must evidently be attained at $V_\mathrm{in} = V_\mathrm{out} = V_\mathrm{in}^0$:

$$g_\mathrm{max} = 2\alpha \sinh\frac{eV_0}{4k_\mathrm{B}T}\sinh\left(\frac{eV_0}{4k_\mathrm{B}T} + c\right)$$
$$\times\,\frac{1}{1+\cosh c}\left\{1 + k_\mathrm{B}T\,\frac{T_\mathrm{b}}{\pi A\Gamma}\left[1 + \cosh\left(\frac{eV_0}{2k_\mathrm{B}T} + c\right)\right]\right\}^{-1}, \tag{19}$$

where $V_0 = V_{\mathrm{ref2}} - V_{\mathrm{ref1}} > 0$ is the power supply voltage. With the background transparency T_b, the value of $g_{\max}$ becomes limited even at high supply voltages. Indeed, for $eV_0/(k_\mathrm{B}T) \gg 1$, Eqn (19) yields

$$g_{\max} \approx \frac{2\pi A\Gamma\alpha}{T_\mathrm{b}(1+\cosh c)k_\mathrm{B}T} \sim \frac{I_\mathrm{on}}{I_\mathrm{off}}\,, \tag{20}$$

where I_on and I_off are the currents flowing through the 'quantum transistors' in the respective open and closed states. The open-state current is proportional to the resonance width and height ($I_\mathrm{on} \sim A\Gamma$); the current in the closed state is determined by the background transparency ($I_\mathrm{off} \sim T_\mathrm{b}$). Thus, by reducing the closed-state current, it is formally possible to increase the absolute value of gain in the inverter indefinitely. However, the background transparency T_b and the resonance width Γ in real structures are related to each other. The former can be qualitatively estimated as the minimum transparency between two widely separated Breit–Wigner resonances,

$$T_\mathrm{b} \approx \frac{4\Gamma^2}{\Delta^2}\,, \tag{21}$$

where $\Delta \gg \Gamma$ is the typical energy separation between resonances. Moreover, the contribution from remote resonances to the current can be disregarded only if they occur outside the effective integration region in Eqn (14), i.e., the condition $\Delta \gg \max(k_\mathrm{B}T, V_{\mathrm{ref2}} - V_{\mathrm{ref1}})$ is satisfied. Taking Eqn (21) into account, we can rewrite Eqn (20) as

$$g_{\max} \approx \frac{\pi A\Delta^2\alpha}{2\Gamma(1+\cosh c)k_\mathrm{B}T}\,. \tag{22}$$

According to this formula, the gain coefficient increases with decreasing Γ, the parameter that characterizes coupling to the contacts. This leads to a decrease both in the resonance width (and hence in the open-state current) and in the background transparency given by Eqn (21) and the closed-state current. At the same time, we note that in addition to beneficial effects associated with a decrease in power consumption and an increase in gain, the reduction in currents can also have an adverse effect on speed: because the tunneling contact resistance behaves as $R \propto \Gamma^{-1}$, the inverter switching time is $\tau = RC \propto \Gamma^{-1}$ (where C is the input capacitance of the device), which increases as Γ decreases. An increase in the separation Δ between neighboring resonances, which leads to a decrease in the background transparency, is also favorable for an increase in gain. According to general formula (19), the conclusion that an increase in the $I_\mathrm{on}/I_\mathrm{off}$ ratio leads to an increase in gain remains valid for supply voltages $V_0 < k_\mathrm{B}T$.

Another way of controlling the transparency of a quantum system is to change the resonance peak height. This effect occurs, for example, in semiconductor resonance-tunneling heterostructures, where the variation of the applied voltage leads to changes in both the shape and height of the potential barriers [87]. It was mentioned in [88] that the resonance amplitude can change as a result of interference effects, but no specific mechanism for this was suggested. The mechanism of resonance collapse in the vicinity of an exceptional point in an open quantum system leading to the coalescence of an even number of unit-transmission resonances and the appearance of a single resonance with a transmission coefficient smaller than unity was considered in [9, 10, 40].

To build a phenomenological model describing the variation in the height of a resonance maximum, in the same spirit as above, we consider narrow resonances that occur on top of some energy-independent background:

$$T_{1,2\mathrm{out}} = T_\mathrm{b} + A_{1,2}\,\frac{4\Gamma^2}{4\Gamma^2 + (E-E_0)^2}\,. \tag{23}$$

Again, we suppose that the value of T_b is small. It is implied in this formula that in contrast to the case described by Eqn (16), the resonance peaks corresponding to the two quantum gates occur at the same energy E_0, which can be made equal to $E_0 = (e/2)(V_{\mathrm{ref1}} + V_{\mathrm{ref2}})$ by the appropriate choice of the reference voltages to ensure a symmetric transfer characteristic. The effect of the input voltage on the resonance height can be phenomenologically described as

$$\begin{aligned} A_1 &= A_{\max}\,\frac{\Gamma^2}{\Gamma^2 + \left[\alpha e(V_\mathrm{in} - V_{\mathrm{ref2}})\right]^2}\,,\\ A_2 &= A_{\max}\,\frac{\Gamma^2}{\Gamma^2 + \left[\alpha e(V_\mathrm{in} - V_{\mathrm{ref1}})\right]^2}\,. \end{aligned} \tag{24}$$

The first factor in Eqns (24) corresponds to the maximal (unit) height of the resonance peak, taking the background contribution to the transparency into account ($A_{\max} = 1 - T_\mathrm{b} \approx 1$). The second factor describes the effect of the input voltage, with $A_{1,2}(V_\mathrm{in} = V_{\mathrm{ref2,1}}) = A_{\max} \approx 1$ and $A_{1,2}(V_\mathrm{in} = V_{\mathrm{ref1,2}}) = \Gamma^2/(\Gamma^2 + \alpha^2 e^2 V_0^2) \ll 1$ for $eV_0 \gg \Gamma$. Phenomenological expression (24) for the resonance amplitude qualitatively describes the effects of both the variation of the barrier transparency [87] and the collapse of resonances [10, 40], which were mentioned in the preceding paragraph.

Writing the condition $I_\mathrm{out} = 0$ similarly to Eqn (17), we can analytically calculate the highest absolute value of the gain coefficient. In the approximation $T_\mathrm{b} \ll 1$, the result is

$$g_{\max} \approx \frac{4k_\mathrm{B}T}{eV_0}\tanh\left(\frac{eV_0}{4k_\mathrm{B}T}\right)\left(2\,\frac{\kappa^2}{1+\kappa^2} - \frac{4k_\mathrm{B}T}{\pi\Gamma}\,T_\mathrm{b}\kappa^2\right), \tag{25}$$

where $\kappa = \alpha eV_0/(4\Gamma)$. According to this formula, the gain in this model is restricted by $g_{\max} < 2$. Thus, the highest gain coefficient exceeds the threshold value required for the functioning of an inverter ($g_\mathrm{th} = 1$). Importantly, in the case of a very weak coupling to the contacts, the inverter can operate at very low supply voltages V_0 if the condition $4\Gamma \ll eV_0 \ll 4k_\mathrm{B}T$ is satisfied. Figure 7 schematically shows the transparency of the quantum systems and the corresponding difference in the distribution functions for input voltages corresponding to the logic 0 and logic 1. The condition $I_\mathrm{out} = 0$ in this case can illustratively be represented as the requirement of proportionality between the peak heights and the differences between the distribution functions calculated at the resonance peak energy.

At the end of this section, we discuss the feasibility and the main features of an inverter design based on controlling antiresonances in quantum transistors. An antiresonance (e.g., a Fano–Feshbach-type resonance) occurs in a quantum system where particles can travel along different interfering paths. Much in the same way as with resonances, an antiresonance can be shifted in energy or eliminated owing to the suppression of destructive interference. Because

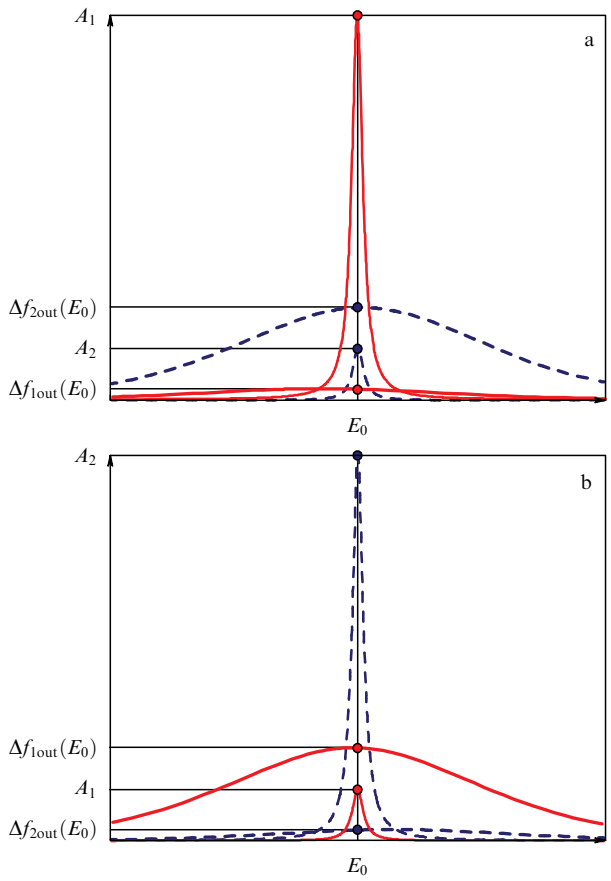

Figure 7. (Color online.) Plots illustrating the condition from which the output voltage of an inverter controlled by the variation in the height of transmission resonances is determined. The two panels correspond to the input voltages of (a) logic 1 ($V_{\text{in}} = V_{\text{ref2}}$) and (b) logic 0 ($V_{\text{in}} = V_{\text{ref1}}$). Thin lines show the transmission coefficients $T_{1\text{out}}$ and $T_{2\text{out}}$ calculated disregarding the 'background' contribution (solid red and dashed blue lines, respectively); thick lines show the differences in the distribution functions $\Delta f_{1\text{out}} = f_{\text{out}} - f_1$ and $\Delta f_{2\text{out}} = f_2 - f_{\text{out}}$ (solid red and dashed blue lines, respectively). If the 'background' transparency is disregarded, the condition of a zero output current can be written as $\Delta f_{1\text{out}}(E_0)A_1 = \Delta f_{2\text{out}}(E_0)A_2$.

antiresonance conditions are determined by the topology of the system, they can be destroyed (without changing the topology or the number of coupled paths) only by introducing additional non-Hermitian channels of coupling of the quantum system to the environment, which leads to the dephasing of the charge-carrier wave functions. One of these methods for controlling antiresonances is described in [89] for a benzene molecule contacted at meta positions. In this case, destructive interference (antiresonance) is suppressed when the molecule is acted upon by a third electrode, which enforces coupling of the molecule to its classical environment and thus leads to the appearance of the imaginary component in the self-energy term. A similar mechanism of controlling the interference transparency was considered in [90] with regard to a Y splitter based on trans-polyacetylene molecules. We note, however, that inasmuch as the molecule is electrically coupled to the control electrode, this design is not truly analogous to an MOS transistor with an (ideally) zero gate current. Rather, it is an analogue of a Schottky-gate transistor, where the gate current is finite even in the ideal case and which is unsuitable for the creation of circuits with a large scale of integration and low power consumption.

Controlling the current through a quantum system by shifting the antiresonance is much less efficient than in the case of resonance. Indeed, the transparency in the vicinity of an isolated antiresonance can be phenomenologically estimated as

$$T(E) \approx \frac{4\Gamma^2(E-E_0)^2}{4\Gamma^2(E-E_0)^2 + \Delta^4}\,, \tag{26}$$

where Δ is the characteristic energy separation from the nearest resonance maximum. Changing the current significantly requires a voltage of the order of the width of the minimum in Eqn (26), which can easily be estimated as $\Delta V \sim \Delta^2/(2\Gamma e\alpha)$. The change in current is proportional to the small value of the background transparency attained far away from the antiresonance minimum:

$$T_{\text{b}} = T(E - E_0 \sim \Delta) \approx \frac{4\Gamma^2}{4\Gamma^2 + \Delta^2} \approx \frac{4\Gamma^2}{\Delta^2} \ll 1\,.$$

At the same time, the interaction of nearby resonances and antiresonances can lead to an improvement in the device characteristics, which is demonstrated in the next subsection.

4.3 Example models of molecular analogues of a CMOS inverter controlled by the shift of resonances or antiresonances

As an example of the simplest implementation of a 'quantum-transistor CMOS inverter,' we consider the structure shown schematically in Fig. 8a. The role of quantum switches is played by the simplest single-site resonance-tunneling systems, each featuring a single resonance (resonance-tunneling transistors):

$$T_{1,2\text{out}}(E) = \frac{4\Gamma^2}{4\Gamma^2 + (E - \varepsilon_{1,2})^2}\,. \tag{27}$$

To calculate the inverter transfer characteristic, we suppose that one of the reference voltages $V_{\text{ref1}} = 0$, and the other is determined by the supply voltage, $V_{\text{ref2}} = V_0$. The electrostatic effect of the input voltage can be described as

$$\begin{aligned} \varepsilon_1 &= \varepsilon_1^0 + \alpha e\left(V_{\text{in}} - \frac{V_0}{2}\right), \\ \varepsilon_2 &= \varepsilon_2^0 + \alpha e\left(V_{\text{in}} - \frac{V_0}{2}\right), \end{aligned} \tag{28}$$

where $\varepsilon_{1,2}^0$ are the energies corresponding to $V_{\text{in}} = V_0/2$. As an example, we consider a system with $\varepsilon_1^0 = -0.025$ eV, $\varepsilon_2^0 = 0.125$ eV, $\Gamma = 0.01$ eV, $\alpha = 0.5$, and the supply voltage $V_0 = 0.1$ V. The transfer characteristic is shown in Fig. 9a. For a higher supply voltage, the transfer characteristic improves; for example, Fig. 9b shows the transfer characteristic for $V_0 = 0.2$ V, $\varepsilon_1^0 = -0.05$ eV, $\varepsilon_0^2 = 0.25$ eV, and the same values of Γ and α.

A more sophisticated example is the structure shown in Fig. 8b. Here, the role of 'quantum transistors' is played by two-site systems, each of them being connected to the respective contact via one of its sites. The transport properties of these systems are characterized by the existence of a Fano–Feshbach-type antiresonance at an energy equal to the energy of the side site [91]. Indeed, following the general method outlined in Section 3 and assuming that quantum systems 1 and 2 in the inverter shown in Fig. 5 represent such

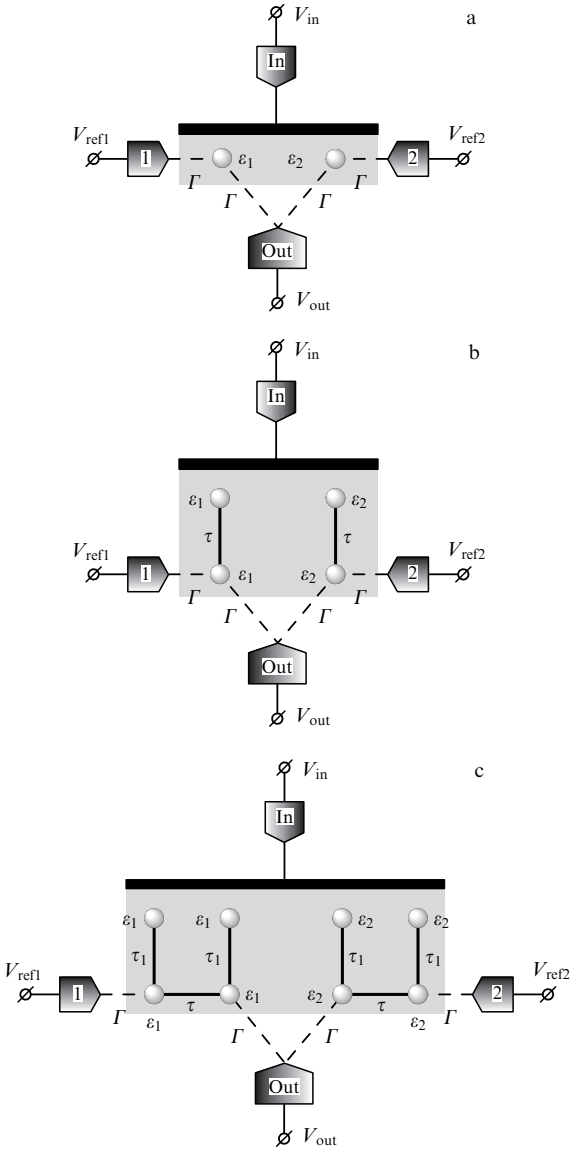

Figure 8. Model quantum-inverter structures based on (a) resonance-tunneling transistors, (b) controlled Fano–Feshbach resonances, and (c) controlled Fano–Feshbach resonances with broad minima. Shading represents the electrostatic effect of the input electrode (the common gate of the inverter).

two-site systems described by the Hamiltonians

$$\hat{H}_{1,2} = \begin{pmatrix} \varepsilon_{1,2} & \tau \\ \tau & \varepsilon_{1,2} \end{pmatrix}, \tag{29}$$

we can calculate the transparencies $T_{1\text{out}}$ and $T_{2\text{out}}$ in the wide-band approximation (disregarding the real parts of self-energy corrections resulting from interaction with the contacts [92]) in the general form [cf. Eqn (11)]:

$$T_{1,2\text{out}}(E) = \frac{P_{1,2\text{out}}^2(E)}{P_{1,2\text{out}}^2(E) + Q_{1,2\text{out}}^2(E)}, \tag{30}$$

where

$$\begin{aligned} P_{1,2\text{out}}(E) &= 2\Gamma(E - \varepsilon_{1,2}), \\ Q_{1,2\text{out}}(E) &= (E - \varepsilon_{1,2})^2 - \tau^2. \end{aligned} \tag{31}$$

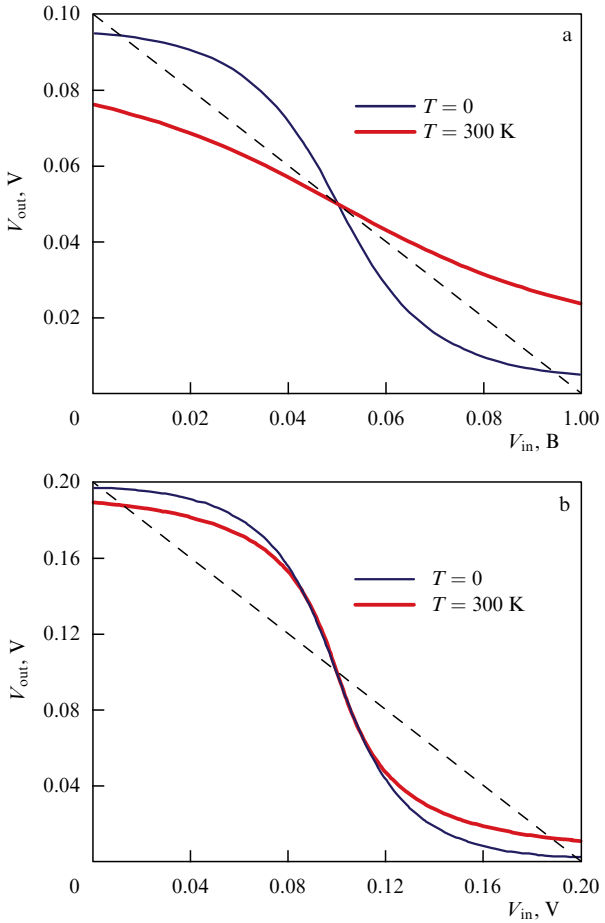

Figure 9. (Color online.) Numerically calculated transfer characteristics of a quantum inverter based on simple single-site quantum switches (Fig. 8a) for supply voltages of (a) 0.1 and (b) 0.2 V. The dashed line shows the critical transfer coefficient −1. The parameters of the structure used in the calculations are listed in the text.

The form of $Q_{1,2\text{out}}$ in Eqn (31) is obtained in accordance with Eqn (12) as the characteristic determinant of the auxiliary Hamiltonian (the input and output are connected to the same site)

$$\hat{H}_{\text{aux}1,2} = \hat{H}_{1,2} + \mathrm{i}\Gamma \begin{pmatrix} 1 & 0 \\ 0 & 0 \end{pmatrix} - \mathrm{i}\Gamma \begin{pmatrix} 1 & 0 \\ 0 & 0 \end{pmatrix} = \hat{H}_{1,2}, \tag{32}$$

where the Hamiltonian $\hat{H}_{1,2}$ is defined by Eqn (29). The value of $P_{1,2\text{out}}$ in this system, where the contacts interact with only one node, is expressed via the minor of the matrix of Hamiltonian (29) obtained by removing the first row and first column [11]. It can be seen from Eqn (30) that the transparencies $T_{1,2\text{out}}$ are equal to unity for $E = \varepsilon_{1,2} \pm \tau$ (the zeros of $Q_{1,2\text{out}}$) and vanish for $E = \varepsilon_{1,2}$ (the zeros of $P_{1,2\text{out}}$). The occurrence of a resonance maximum near the antiresonance in these quantum switches improves the characteristics of the device owing to the effective suppression of the background contribution to the transparency in the presence of an antiresonance.

The effect of the potential at the input electrode in this system can be described similarly to Eqn (28). It is easy to pick an exemplary set of parameters for which the optimum transfer characteristic of the system (at zero temperature) are realized. We consider a system with $\Gamma = 0.01$ eV, $\alpha = 0.5$, the supply voltage $V_0 = 0.1$ V, $\varepsilon_1^0 = (eV_0/2)(1+\alpha) = 0.075$ eV, $\varepsilon_2^0 = (eV_0/2)(1-\alpha) = 0.025$ eV, and $\tau = eV_0 = 0.1$ eV. This

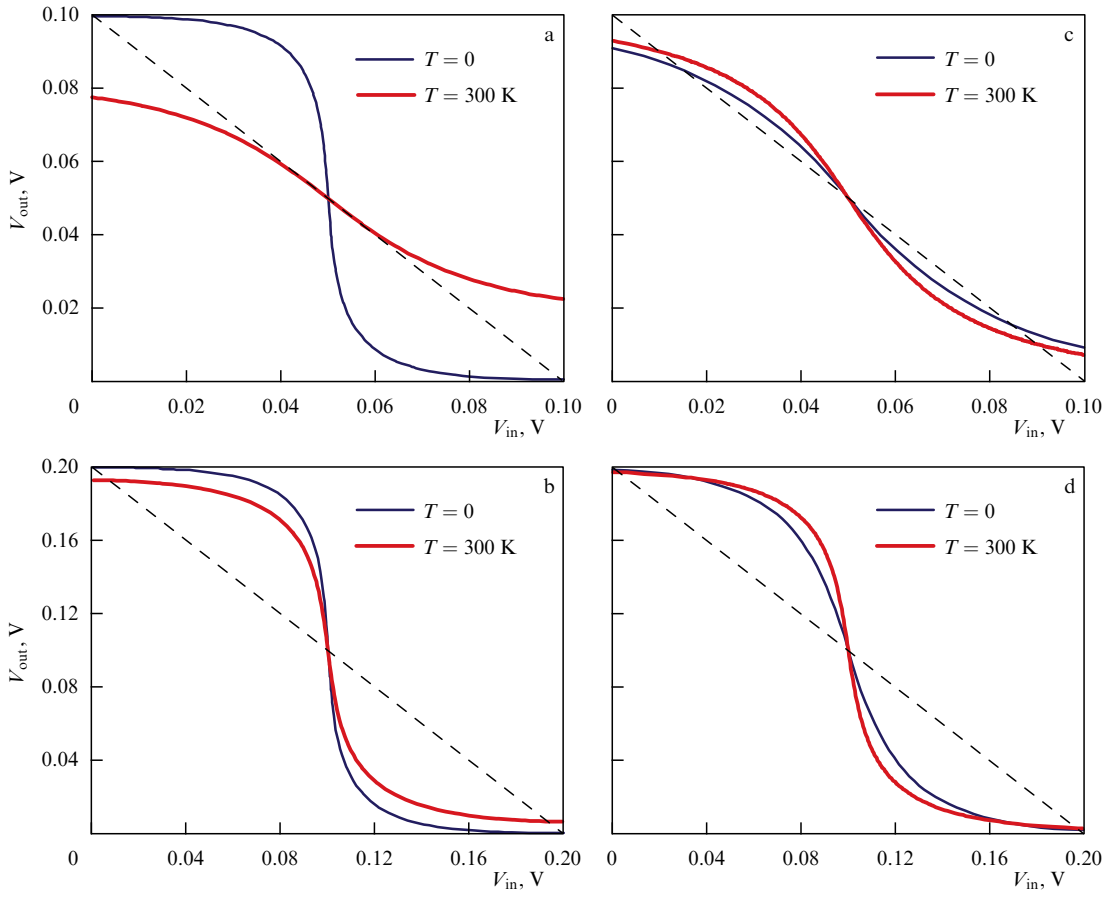

Figure 10. (Color online.) Numerically calculated transfer characteristics of a quantum inverter based on two-site quantum systems for supply voltages of (a), (c) 0.1 and (b), (d) 0.2 V. The dashed line shows the critical transfer coefficient -1. The parameters of the structure used in the calculations are listed in the text.

choice of parameters ensures a maximum in the transparency $T_{1\text{out}}$ at the energy $E = eV_{\text{ref1}} = 0$ for the input voltage $V_{\text{in}} = V_{\text{ref2}} = V_0$ and a maximum of $T_{2\text{out}}$ at the energy $E = eV_{\text{ref2}} = eV_0$ for $V_{\text{in}} = V_{\text{ref1}} = 0$. At the same time, the background values of the transparencies are effectively reduced owing to the presence of antiresonances in $T_{1\text{out}}$ and $T_{2\text{out}}$ in the energy range between 0 and eV_0. The transfer characteristic for this case is plotted in Fig. 10a. The transfer characteristic for a similar system with the supply voltage $V_0 = 0.2$ V is shown in Fig. 10b. However, it is possible to select the parameters of the system such that room-temperature characteristics are superior to zero-temperature ones. For example, the transfer characteristic for a system with $\varepsilon_1^0 = 0.15$ eV, $\varepsilon_2^0 = -0.05$ eV, $\tau = 0.25$ eV, $\Gamma = 0.01$ eV, $\alpha = 0.5$, and the supply voltage $V_0 = 0.1$ V is plotted in Fig. 10c. Figure 10d shows the transfer characteristic for a higher supply voltage $V_0 = 0.2$ V with $\varepsilon_1^0 = 0.275$ eV, $\varepsilon_2^0 = -0.075$ eV, $\tau = 0.35$ eV, and the same values of Γ and α.

In the same way, we can calculate the model transfer characteristic of an inverter with even more complex quantum systems (Fig. 8c) that have broader resonances and antiresonances owing to their coalescence, described in detail in [11]. In this case, the quantum systems playing the role of electric switches are described by the Hamiltonians

$$\hat{H}_{1,2} = \begin{pmatrix} \varepsilon_{1,2} & \tau_1 & \tau & 0 \\ \tau_1 & \varepsilon_{1,2} & 0 & 0 \\ \tau & 0 & \varepsilon_{1,2} & \tau_1 \\ 0 & 0 & \tau_1 & \varepsilon_{1,2} \end{pmatrix}, \tag{33}$$

whence it is easy to obtain the corresponding transmission coefficients in form (30), but with different expressions for $P_{1,2\text{out}}$ and $Q_{1,2\text{out}}$:

$$\begin{aligned} P_{1,2\text{out}}(E) &= 2\Gamma\tau(E - \varepsilon_{1,2})^2, \\ Q_{1,2\text{out}}(E) &= (E - \varepsilon_{1,2})^4 + (E - \varepsilon_{1,2})^2(\Gamma^2 - \tau^2 - 2\tau_1^2) + \tau^4. \end{aligned} \tag{34}$$

The auxiliary Hamiltonian for the calculation of $Q_{1,2\text{out}}$ is

$$\begin{aligned} \hat{H}_{\text{aux}1,2} &= \hat{H}_{1,2} + \mathrm{i}\Gamma \begin{pmatrix} 1 & 0 & 0 & 0 \\ 0 & 0 & 0 & 0 \\ 0 & 0 & 0 & 0 \\ 0 & 0 & 0 & 0 \end{pmatrix} - \mathrm{i}\Gamma \begin{pmatrix} 0 & 0 & 0 & 0 \\ 0 & 0 & 0 & 0 \\ 0 & 0 & 1 & 0 \\ 0 & 0 & 0 & 0 \end{pmatrix} \\ &= \begin{pmatrix} \varepsilon_{1,2} + \mathrm{i}\Gamma & \tau_1 & \tau & 0 \\ \tau_1 & \varepsilon_{1,2} & 0 & 0 \\ \tau & 0 & \varepsilon_{1,2} - \mathrm{i}\Gamma & \tau_1 \\ 0 & 0 & \tau_1 & \varepsilon_{1,2} \end{pmatrix}, \end{aligned} \tag{35}$$

with $\hat{H}_{1,2}$ given by Eqn (33). The functions $P_{1,2\text{out}}$ are again calculated via the minor of Hamiltonian (33), because each contact interacts with only one site in the system [11]. The structure shown in Fig. 8c has broader antiresonances than those featured by the structure shown in Fig. 8c, because the roots of $P_{1,2\text{out}}$ have a higher multiplicity. The effect of a potential applied to the input electrode on the on-site energies is described similarly to Eqn (28). The transfer characteristics calculated for the supply voltages $V_0 = 0.1$ and 0.2 V are plotted in Fig. 11. Evidently, the gain coefficient in this case is much higher than that for a simpler structure. The following

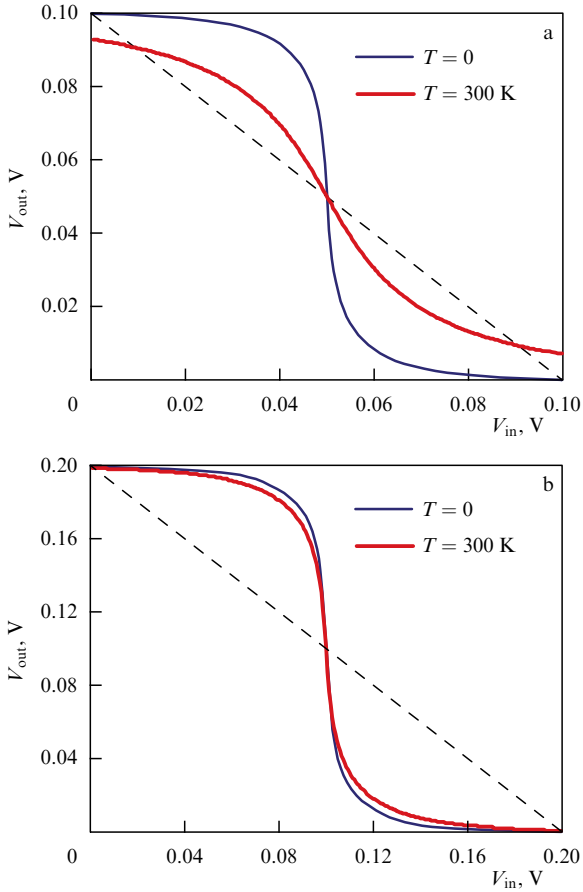

Figure 11. (Color online.) Numerically calculated transfer characteristics of a quantum interference inverter based on four-site quantum systems for supply voltages of (a) 0.1 and (b) 0.2 V. The dashed line shows the critical transfer coefficient -1. The parameters of the structure used in the calculations are listed in the text.

parameters were used in these calculations: $\varepsilon_1^0 = 0.1$ eV, $\varepsilon_2^0 = 0$, $\tau = 0.1$ eV, $\tau_1 = 0.2$ eV, $\Gamma = 0.01$ eV, and $\alpha = 0.5$ for $V_0 = 0.1$ V and $\varepsilon_1^0 = 0.2$ eV, $\varepsilon_2^0 = 0$, $\tau = 0.225$ eV, $\tau_1 = 0.375$ eV, $\Gamma = 0.01$ eV, and $\alpha = 0.5$ for $V_0 = 0.2$ V.

Thus, we have demonstrated in this section that quantum analogues of CMOS inverters can be constructed on the basis of the simplest quantum structures featuring both resonances and antiresonances, and outlined ways to optimize their parameters and characteristics.

5. Conclusions

In recent years, there has been a surge in interest in quantum technologies. The quantum analogues of CMOS gates considered is this paper offer an example of how quantum principles can be employed in the development of the traditional integrated circuit (IC) basic components implementing Boolean functions to perform calculations in the framework of the approach dating back to von Neumann.

The swift progress in modern information technologies is underlain primarily by advances in the traditional IC basic components. Even if quantum computers, which rely on entirely different principles involving entangled states of quantum bits (qubits), are ever created, they will find application for a quite limited range of problems, leaving a very broad field to traditional computers. Within the next few decades, the nominal computing capacity of traditional systems (which can roughly be estimated as the number of logic gates on a chip) will match that of the human brain, which opens extraordinarily broad prospects for studies on artificial intelligence and can radically change our lives.

We emphasize that the molecular quantum gates discussed in Section 4 are composed of elements representing, in fact, quantum field-effect transistors, and can therefore be used for building computers with architectures different from von Neuman's, which further expands their possible application area. The key requirement for the implementation of molecular gates is the advent of atomic-precision lithography techniques. If such a technology is developed (to which huge effort and resources are currently targeted), the broad adoption of the molecular IC basic components will become almost inevitable. We note that by 'molecule' we mean any chemically stable object with dimensions of the order of one or several nanometers and having a discrete energy spectrum. The investigation of the properties of such objects, and coherent quantum transport in the first place, as well as the principles and rules for designing and building computer systems based on these elements, is a very important problem in the development of the IC basic components of information technologies.

This study was carried out in the framework of a state assignment for the Lebedev Physical Institute, Russian Academy of Sciences, and was supported in part by the Presidium of the Russian Academy of Sciences.

References

1. Hu C C *Modern Semiconductor Devices for Integrated Circuits* (Upper Saddle River, NJ: Prentice Hall, 2010)
2. Horowitz P, Hill W *The Art of Electronics* (Cambridge: Cambridge Univ. Press, 1989)
3. Gorbatsevich A A et al. *Phys. Low-Dim. Struct.* (4) 5 (1994)
4. Gorbatsevich A A et al. *Mikroelektronika* **23** 17 (1994)
5. Gorbatsevich A A et al. *Elektron. Promyshlennost* (4) 28 (1995)
6. Gorbatsevich A A, Kapaev V V, Kopaev, Yu V *JETP* **80** 734 (1995); *Zh. Eksp. Teor. Fiz.* **107** 1320 (1995)
7. Prince B *Vertical 3D Memory Technologies* (Chichester: John Wiley and Sons, 2014)
8. International Technology Roadmap for Semiconductors 2015, http://www.itrs2.net/
9. Gorbatsevich A A, Shubin N M *JETP Lett.* **103** 769 (2016); *Pis'ma Zh. Eksp. Teor. Fiz.* **103** 866 (2016)
10. Gorbatsevich A A, Shubin N M *Ann. Physics* **376** 353 (2017)
11. Gorbatsevich A A, Shubin N M *Phys. Rev. B* **96** 205441 (2017)
12. Landau L D, Lifshitz E M *Quantum Mechanics: Non-Relativistic Theory* Vol. 3 (Oxford: Elsevier, 2013); Translated from Russian: *Kvantovaya Mekhanika: Nerelyativistskaya Teoriya* Vol. 3 (Moscow: Fizmatlit, 2013)
13. Lindblad G *Commun. Math. Phys.* **48** 119 (1976)
14. Brasil C A, Fanchini F F, R Napolitano R de J *Rev. Bras. Ensino Fís.* **35** (1) 01 (2013)
15. Kurobe A et al. *Semicond. Sci. Technol.* **9** 1744 (1994)
16. Birjulin P I et al. *Semicond. Sci. Technol.* **12** 427 (1997)
17. Valiev K A *Phys. Usp.* **48** 1 (2005); *Usp. Fiz. Nauk* **175** 3 (2005)
18. Joachim C, Renaud N, Hliwa M *Adv. Mater.* **24** 312 (2012)
19. Hatano N et al. *Prog. Theor. Phys.* **119** 187 (2008)
20. Feshbach H *Ann. Physics* **5** 357 (1958)
21. Feshbach H *Ann. Physics* **19** 287 (1962)
22. Feshbach H *Ann. Physics* **43** 410 (1967)
23. Siegert A J F *Phys. Rev.* **56** 750 (1939)
24. Sasada K, Hatano N, Ordonez G *J. Phys. Soc. Jpn.* **80** 104707 (2011)
25. Fano U *Phys. Rev.* **124** 1866 (1961)
26. Mies F H, Krauss M *J. Chem. Phys.* **45** 4455 (1966)
27. Mies F H *Phys. Rev.* **175** 164 (1968)
28. Moldauer P A *Phys. Rev. Lett.* **18** 249 (1967)
29. Müller M et al. *Phys. Rev. E* **52** 5961 (1995)

30. Persson E, Rotter I *Phys. Rev. C* **59** 164 (1999)
31. Persson E et al. *Phys. Rev. Lett.* **85** 2478 (2000)
32. Moiseyev N *Non-Hermitian Quantum Mechanics* (Cambridge: Cambridge Univ. Press, 2011)
33. Miroshnichenko A E, Flach S, Kivshar Yu S *Rev. Mod. Phys.* **82** 2257 (2010)
34. Monticone F, Alù A *Rep. Prog. Phys.* **80** 36401 (2017)
35. Hsu C W et al. *Nature Rev. Mater.* **1** 16048 (2016)
36. Breit G, Wigner E *Phys. Rev.* **49** 519 (1936)
37. Klaiman S, Moiseyev N *J. Phys. B* **43** 185205 (2010)
38. Romo R, García-Calderón G *Phys. Rev. B* **49** 14016 (1994)
39. Dragunov V P, Neizvestnyi I G, Gridchin V A *Osnovy Nanoelektroniki* (Fundamentals of Nanoelectronics) (Moscow: Logos, 2006)
40. Gorbatsevich A A, Zhuravlev M N, Kapaev V V *JETP* **107** 288 (2008); *Zh. Eksp. Teor. Fiz.* **134** 338 (2008)
41. Vanroose W et al. *J. Phys. A* **30** 5543 (1997)
42. Vanroose W et al. *Phys. Rev. A* **64** 62708 (2001)
43. Heiss W D, Wunner G *Eur. Phys. J. D* **68** 284 (2014)
44. Ambichl P et al. *Phys. Rev. X* **3** 041030 (2013)
45. Chong Y D, Ge L, Stone A D *Phys. Rev. Lett.* **106** 93902 (2011)
46. Aharonov Y, Bohm D *Phys. Rev.* **115** 485 (1959)
47. Bender C M, Boettcher S *Phys. Rev. Lett.* **80** 5243 (1998)
48. Bender C M, Boettcher S, Meisinger P N *J. Math. Phys.* **40** 2201 (1999)
49. Bender C M *Rep. Prog. Phys.* **70** 947 (2007)
50. Mostafazadeh A *J. Math. Phys.* **43** 205 (2002)
51. Mostafazadeh A *J. Math. Phys.* **43** 2814 (2002)
52. Mostafazadeh A *J. Math. Phys.* **43** 3944 (2002)
53. Zyablovsky A A et al. *Phys. Usp.* **57** 1063 (2014); *Usp. Fiz. Nauk* **184** 1177 (2014)
54. Eleuch H, Rotter I *Eur. Phys. J. D* **69** 229 (2015)
55. Eleuch H, Rotter I *Eur. Phys. J. D* **69** 230 (2015)
56. Kato T *Perturbation Theory for Linear Operators* (Berlin: Springer, 1995)
57. Mandal I *Europhys. Lett.* **110** 67005 (2015)
58. San-Jose P et al. *Sci. Rep.* **6** 21427 (2016)
59. Kreibich M et al. *Phys. Rev. A* **87** 051601(R) (2013)
60. Chtchelkatchev N M et al. *Phys. Rev. Lett.* **109** 150405 (2012)
61. Guo A et al. *Phys. Rev. Lett.* **103** 093902 (2009)
62. Regensburger A et al. *Nature* **488** 167 (2012)
63. Bittner S et al. *Phys. Rev. Lett.* **108** 24101 (2012)
64. Alaeian H, Dionne J A *Phys. Rev. A* **89** 33829 (2014)
65. Mostafazadeh A *Ann. Physics* **368** 56 (2016)
66. Liertzer M et al. *Phys. Rev. Lett.* **108** 173901 (2012)
67. Brandstetter M et al. *Nature Commun.* **5** 4034 (2014)
68. Landau L D, Lifshitz E M *Electrodynamics of Continuous Media* (Oxford: Elsevier, 2013); Translated from Russian: *Elektrodinamika Sploshnykh Sred* (Moscow: Fizmatlit, 2003)
69. Zyablovsky A A et al. *Phys. Rev. A* **89** 33808 (2014)
70. Cannata F, Dedonder J-P, Ventura A *Ann. Physics* **322** 397 (2007)
71. Jin L, Song Z *Phys. Rev. A* **81** 32109 (2010)
72. Jin L, Song Z *J. Phys. A* **44** 375304 (2011)
73. Hernandez-Coronado H, Krejčiřík D, Siegl P *Phys. Lett. A* **375** 2149 (2011)
74. Datta S *Electronic Transport in Mesoscopic Systems* (Cambridge: Cambridge Univ. Press, 1997)
75. Büttiker M *Phys. Rev. Lett.* **57** 1761 (1986)
76. Theis T N, Solomon P M *Proc. IEEE* **98** 2005 (2010)
77. Ionescu A M, Riel H *Nature* **479** 329 (2011)
78. Celardo G L, Kaplan L *Phys. Rev. B* **79** 155108 (2009)
79. Celardo G L et al. *Phys. Rev. B* **82** 165437 (2010)
80. Nitzan A, Ratner M A *Science* **300** 1384 (2003)
81. Kergueris C et al. *Phys. Rev. B* **59** 12505 (1999)
82. Papadopoulos T A, Grace I M, Lambert C J *Phys. Rev. B* **74** 193306 (2006)
83. Kaasbjerg K, Flensberg K *Nano Lett.* **8** 3809 (2008)
84. Osorio E A et al. *Nano Lett.* **7** 3336 (2007)
85. Puczkarski P et al. *Appl. Phys. Lett.* **107** 133105 (2015)
86. Perrin M L et al. *Nature Nanotechnol.* **8** 282 (2013)
87. Mizuta H, Tanoue T *The Physics and Applications of Resonant Tunnelling Diodes* (Cambridge: Cambridge Univ. Press, 2006)
88. Li Y et al. *Sci. Rep.* **6** 33686 (2016)
89. Stafford C A, Cardamone D M, Mazumdar S *Nanotechnology* **18** 424014 (2007)
90. Gorbatsevich A A, Zhuravlev M N, Kataeva T S *Russ. Microelectronics* **46** 414 (2017); *Mikroelektronika* **46** 451 (2017)
91. Miroshnichenko A E, Kivshar Yu S *Phys. Rev. E* **72** 056611 (2005)
92. Dente A D, Bustos-Marún R A, Pastawski H M *Phys. Rev. A* **78** 062116 (2008)